International Journal of Heat and Fluid Flow 30 (2009) 229–236

Contents lists available at ScienceDirect

International Journal of Heat and Fluid Flow

journal homepage: www.elsevier.com/locate/ijhff

Effect of thermal dispersion on free convection in a fluid saturated porous medium

Ibrahim A. Abbas [a,*], M.F. El-Amin [b], Amgad Salama [c,1]

[a] Mathematics Department, Faculty of Science, Sohag University, Sohag 82524, Egypt
[b] Mathematics Department, Aswan Faculty of Science, South Valley University, Aswan 81258, Egypt
[c] Environmental Engineering Department, Konkuk University, Seoul 143-701, South Korea

ARTICLE INFO

Article history:
Received 22 February 2008
Received in revised form 13 January 2009
Accepted 16 January 2009
Available online 23 February 2009

Keywords:
Porous medium
Thermal dispersion
Natural convection
Finite element method

ABSTRACT

The present article considers a numerical study of thermal dispersion effect on the non-Darcy natural convection over a vertical flat plate in a fluid saturated porous medium. Forchheimer extension is considered in the flow equations. The coefficient of thermal diffusivity has been assumed to be the sum of molecular diffusivity and the dispersion thermal diffusivity due to mechanical dispersion. The non-dimensional governing equations are solved by the finite element method (FEM) with a Newton–Raphson solver. Numerical results for the details of the stream function, velocity and temperature contours and profiles as well as heat transfer rates in terms of Nusselt number are obtained. The study shows that the increase in thermal dispersion coefficient of the porous medium results in more heat energy to disperse away in the normal direction to the wall. This induces more fluid to flow along the wall, enhancing the heat transfer coefficient particularly near the wall.

1. Introduction

Transport phenomena in porous media have challenged engineers and researchers for quite a bit of time in trying to adopt the appropriate framework within which solution may be attained. The pioneering work of Henri Darcy on this issue opened the road towards the understanding of the main essence of the subject. That is, we do not need detailed descriptions of the motion of the fluid within the pore structure, and even if we are able to get it we would, for the sake of our engineering applications, integrate the details to get some useful quantities. It has been realized by the late seventies of the last century that we may adopt the continuum hypothesis to transport phenomena in porous media through upscaling processes. To adopt the continuum approach to phenomena occurring in highly complex and even unknown structure implies that the primary variables of interest or its derivatives that may suffer of discontinuities at the interface between the fluid body and the solid grains of the porous media may be replaced by other variables that are continuous everywhere in the domain. This would lead us to substantially decrease the number of degrees of freedom of the system and hence made it amenable to mathematical manipulations. However, to correctly adopt the continuum hypothesis to transport phenomena in porous media, certain conditions and length scale constraints need to be satisfied. Failing to satisfy these conditions would result in the inappropriateness of the continuum hypothesis and other sophisticated methods need to be adopted (Salama and Van Geel, 2008).

Yet for all the simplifications that it made, the continuum hypothesis as applied to transport phenomena in porous media has confronted some difficulties that entailed the introduction of some constitutive relationships to account for the apparent differences between the upscaled and the actual variables. To give an example, the actual velocity of fluid particles within the pore structures changes significantly between zero at the interface and different than zero within the pores, whereas within the continuum hypothesis the upscaled velocity may be constant or at most changes, comparatively, slowly. This would result in the existence of additional mass and/or energy fluxes. It has thus been hypothesized that these additional fluxes may be accounted for by adding terms to their respective flux terms that may be assumed to depend on the upscaled velocity. Thus, in terms of solute transport, the usual diffusion mechanism has been augmented by another mechanism that is called mass dispersion term which depends on the upscaled velocity. Likewise, energy transport (like heat transport) in porous media required the addition of a thermal dispersion mechanism to the usual thermal diffusion mechanism.

In this study, we consider the effect of thermal dispersion mechanism on the development of the thermally-driven convection boundary layer flow in porous media. This subject is of considerable interest in a variety of engineering applications including geothermal energy technology, petroleum recovery, filtration processes, packed bed reactors and underground disposal of chemical and nuclear waste.

Similarity solution for the Darcian regime with no dispersion has been presented by Cheng and Minkowycz (1977). The

* Corresponding author.
E-mail addresses: ibrabbas7@yahoo.com (I.A. Abbas), mfam2000@yahoo.com (M.F. El-Amin), asalama@konkuk.ac.kr (A. Salama).
[1] Permanent Address: Nuclear Research Center. AEA, Abu-Zabal 13759, Egypt.

0142-727X/$ - see front matter © 2009 Elsevier Inc. All rights reserved.
doi:10.1016/j.ijheatfluidflow.2009.01.004

Nomenclature

A	constant
C	empirical constant
d	pore diameter
g	gravitational constant
K	permeability of the porous medium
k_d	dispersion thermal conductivity
k_e	effective thermal conductivity
Nu_x	local Nusselt number
p	pressure
q	local heat flux
Ra	Rayleigh number
$\overline{T}$	temperature
T	non-dimensional temperature
$\overline{u}, \overline{v}$	velocity components in the $\overline{x}$ and $\overline{y}$ directions
u, v	non-dimensional velocity components in the x and y directions
$\overline{x}, \overline{y}$	Cartesian coordinates
x, y	non-dimensional Cartesian coordinates
ρ	fluid density
μ	viscosity
ν	fluid kinematic viscosity
α	molecular thermal diffusivity
α_d	dispersion diffusivity
α_x, α_y	thermal diffusion coefficients in x and y directions respectively
β	thermal expansion coefficient
γ	mechanical dispersion coefficient
ψ	dimensional stream function
Subscripts	
w	evaluated on the wall
∞	evaluated at the outer edge of the boundary layer

dependence of heat dispersion on the upscaled velocity has been proposed by several investigators to be linear (e.g., Fried and Combarnous (1976), Georgiadis and Catton (1988), Cheng (1981) and Plumb (1983)). On the other hand, an analysis of the effect of thermal dispersion on vertical plate natural convection in porous media is presented by Hong and Tien (1987). Lai and Kulacki (1989) investigated the effect of thermal dispersion on the non-Darcy convection from a horizontal surface submerged in saturated porous media. The effects of thermal dispersion and lateral mass flux on non-Darcy natural convection over a vertical flat plate in a fluid saturated porous medium were studied by Murthy and Singh (1997). Mansour and El-Amin (1999) studied the effects of thermal dispersion on non-Darcy axisymmetric free convection in a saturated porous medium with lateral mass transfer. El-Amin (2004) investigated the effects of double dispersion on natural convection heat and mass transfer in non-Darcy porous medium. The problem of thermal dispersion effects on non-Darcy axisymmetric free convection in a power-law fluid saturated porous medium was studied by El-Amin (2005).

The present investigation is devoted to study the effect of thermal dispersion on Forchheimer natural convection over a vertical flat plate in a fluid saturated porous medium. The coefficient of thermal diffusivity is assumed to be the sum of molecular diffusivity and the dispersion thermal diffusivity due to mechanical dispersion. The wall temperature distribution is assumed to be uniform. The non-dimensional equations are solved using the FEM.

2. Analysis

Let us consider the non-Darcy natural convection flow and heat transfer over a semi infinite vertical surface in a fluid saturated porous medium, Fig. 1. The governing equations for this problem are given by

$$\frac{\partial \overline{u}}{\partial \overline{x}} + \frac{\partial \overline{v}}{\partial \overline{y}} = 0 \tag{1}$$

$$\overline{u} + \frac{C\sqrt{K}}{\nu}\overline{u}q = -\frac{K}{\mu}\left(\frac{\partial p}{\partial \overline{x}} + \rho g\right) \tag{2}$$

$$\overline{v} + \frac{C\sqrt{K}}{\nu}\overline{v}q = -\frac{K}{\mu}\left(\frac{\partial p}{\partial \overline{y}}\right) \tag{3}$$

$$\overline{u}\frac{\partial \overline{T}}{\partial \overline{x}} + \overline{v}\frac{\partial \overline{T}}{\partial \overline{y}} = \frac{\partial}{\partial \overline{x}}\left(\alpha_{\overline{x}}\frac{\partial \overline{T}}{\partial \overline{x}}\right) + \frac{\partial}{\partial \overline{y}}\left(\alpha_{\overline{y}}\frac{\partial \overline{T}}{\partial \overline{y}}\right) \tag{4}$$

$$\rho = \rho_\infty[1 - \beta(\overline{T} - \overline{T}_\infty)] \tag{5}$$

where $q^2 = \overline{u}^2 + \overline{v}^2$ along with the boundary conditions

$$\begin{aligned} &\overline{y} = 0 : \overline{v} = 0, \quad \overline{T}_w = const. \\ &\overline{y} \to \infty : \overline{u} = 0, \quad \overline{T} \to \overline{T}_\infty \end{aligned} \tag{6}$$

where $\overline{u}$ [L/T] and $\overline{v}$ [L/T] are the velocity components in the $\overline{x}$ and $\overline{y}$ -directions, respectively, $(\rho_\infty C_p)_f$ is the product of density [M/L^3] and specific heat of the fluid [L^2/KT^2], p is the pressure [M/LT^2], $\overline{T}$ is the temperature [K], K [L^2] is the permeability constant, C is an empirical constant, dimensionless, β is the thermal expansion coefficient [1/K], μ is the viscosity of the fluid [M/LT], g is the acceleration due to gravity [L/T^2], $\alpha_{\overline{x}}$ and $\alpha_{\overline{y}}$ are the components of the thermal diffusivity in $\overline{x}$ and $\overline{y}$ directions respectively [L^2/T]. The normal component of the velocity near the boundary is considered small compared with the vertical component and the derivatives of any quantity in the normal direction to the wall are large compared with derivatives of the quantity in the direction of the wall (i.e., the vertical direction). Under these assumptions Eqs. (1)–(5) become:

$$\frac{\partial \overline{u}}{\partial \overline{x}} + \frac{\partial \overline{v}}{\partial \overline{y}} = 0 \tag{7}$$

$$\overline{u} + \frac{C\sqrt{K}}{\nu}\overline{u}|\overline{u}| = -\frac{K}{\mu}\left(\frac{\partial p}{\partial \overline{x}} + \rho g\right) \tag{8}$$

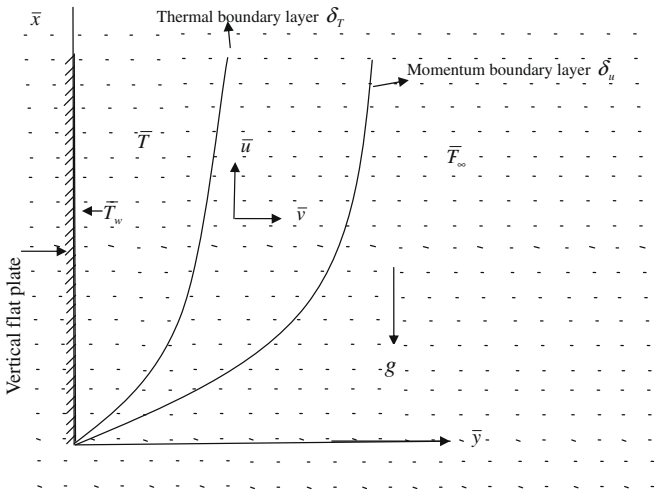

Fig. 1. Physical model and coordinate system.

$$\frac{\partial p}{\partial \overline{y}} = 0 \tag{9}$$

$$\overline{u}\frac{\partial \overline{T}}{\partial \overline{x}} + \overline{v}\frac{\partial \overline{T}}{\partial \overline{y}} = \frac{\partial}{\partial \overline{y}}\left(\alpha_{\overline{y}}\frac{\partial \overline{T}}{\partial \overline{y}}\right) \tag{10}$$

The quantity $\alpha_{\overline{y}}$ is variable and is defined as the sum of molecular thermal diffusivity α and dispersion thermal diffusivity α_d. Following Plumb (1983), we assume the dispersion thermal diffusivity as to linearly change with the upscaled velocity such that, $\alpha_d = \gamma|\overline{u}|d$, where γ is the mechanical dispersion coefficient whose value depends on the structure of the porous media and d is the pore diameter.

Invoking the Boussinesq approximations, by substituting Eq. (5) into Eq. (9), and with some mathematical manipulations, the pressure term can be eliminated and the velocity components u and v can be written in terms of stream function $\overline{\psi}$ as: $\overline{u} = \partial\overline{\psi}/\partial\overline{y}$ and $\overline{v} = -\partial\overline{\psi}/\partial\overline{x}$, we obtain:

$$\frac{\partial^2\overline{\psi}}{\partial\overline{y}^2} + \frac{C\sqrt{K}}{\nu}\frac{\partial}{\partial\overline{y}}\left(\frac{\partial\overline{\psi}}{\partial\overline{y}}\right)^2 = \frac{Kg\beta}{\nu}\frac{\partial\overline{T}}{\partial\overline{y}} \tag{11}$$

$$\frac{\partial\overline{\psi}}{\partial\overline{y}}\frac{\partial\overline{T}}{\partial\overline{x}} - \frac{\partial\overline{\psi}}{\partial\overline{x}}\frac{\partial\overline{T}}{\partial\overline{y}} = \frac{\partial}{\partial\overline{y}}\left[(\alpha+\alpha_d)\frac{\partial\overline{T}}{\partial\overline{y}}\right] \tag{12}$$

Introducing the non-dimensional transformations:

$$y = \overline{y}/d, x = \overline{x}/d, \psi = \overline{\psi}/\alpha, T = (\overline{T} - \overline{T}_\infty)/(\overline{T}_w - \overline{T}_\infty) \tag{13}$$

The problem statement then becomes:

$$\frac{\partial^2\psi}{\partial y^2} + 2F_0\frac{\partial\psi}{\partial y}\frac{\partial^2\psi}{\partial y^2} = Ra\frac{\partial T}{\partial y} \tag{14}$$

$$\frac{\partial\psi}{\partial y}\frac{\partial T}{\partial x} - \frac{\partial\psi}{\partial x}\frac{\partial T}{\partial y} = \frac{\partial}{\partial y}\left[\left(1+\gamma\frac{\partial\psi}{\partial y}\right)\frac{\partial T}{\partial y}\right] \tag{15}$$

Table 1
Grid independent test (R_{ad} = 10, γ = 0.5, F_0 = 0.5, x = 10, y = 10).

Mesh size	ψ	T
10 × 10	1.181790E+001	1.507303E−001
20 × 20	1.234669E+001	2.080401E−001
30 × 30	1.251212E+001	2.240477E−001
40 × 40	1.259287E+001	2.318501E−001
50 × 50	1.264069E+001	2.364608E−001
60 × 60	1.267229E+001	2.395064E−001
70 × 70	1.269473E+001	2.416684E−001

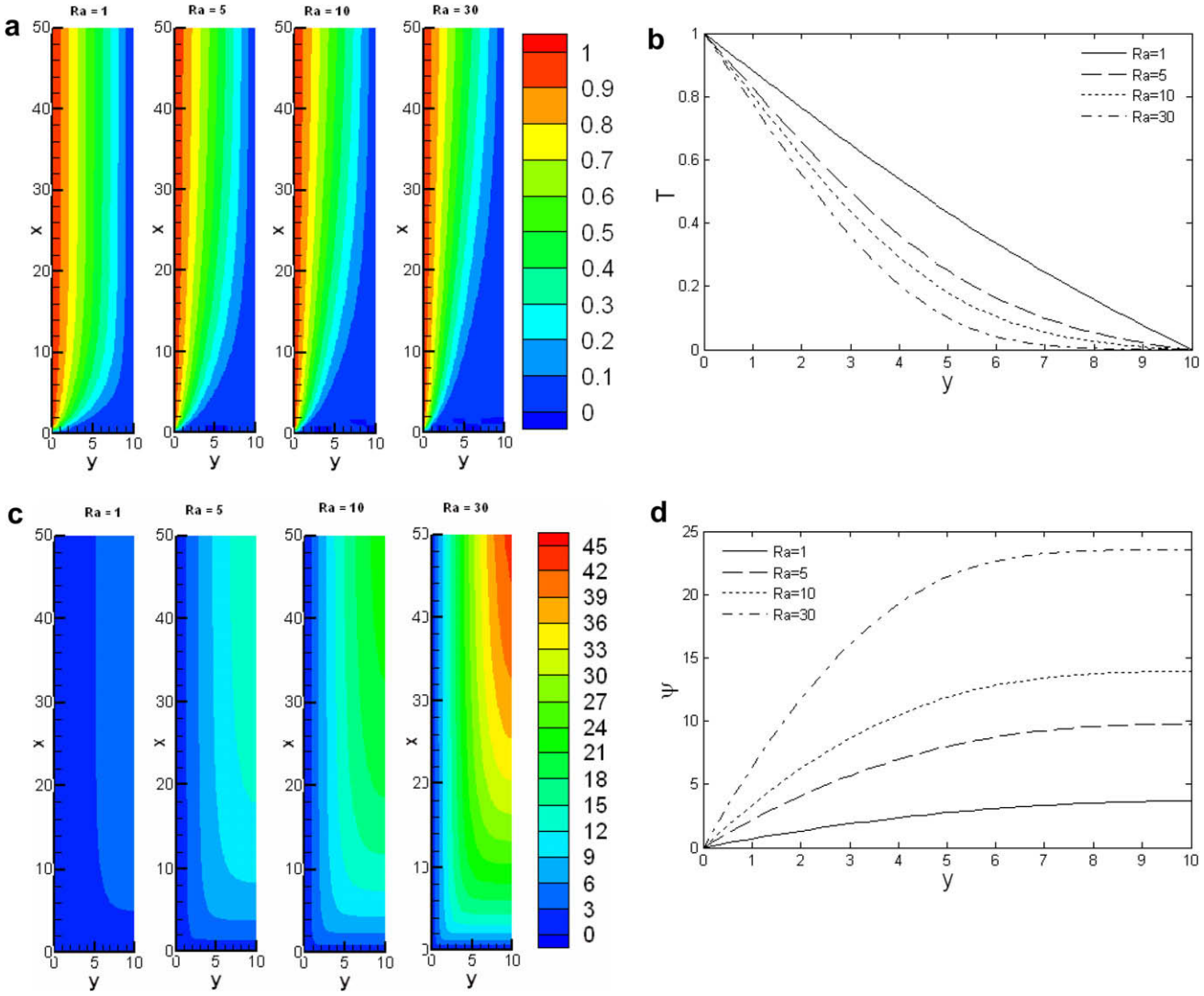

Fig. 2. (a) Temperature contours for various values of *Ra* at F_0 = 0.5 and γ = 0.3. (b) Temperature profiles for various values of *Ra* with F_0 = 0.5 and γ = 0.3 at x = 10. (c) Stream function contours as a function of y for various values of *Ra* at F_0 = 0.5 and γ = 0.3. (d) Stream function profiles as a function of y for various values of *Ra* at F_0 = 0.5 and γ = 0.3. (e) Velocity contours for various values of *Ra* with F_0 = 0.5 and γ = 0.3 at x = 10. (f) Velocity profiles for various values of *Ra* with F_0 = 0.5 and γ = 0.3 at x = 10. (g) Nusselt number as a function of x for various values of *Ra* with F_0 = 0.5 and γ = 0.3.

Along with the boundary conditions

$$y = 0 : \partial\psi/\partial x = 0, \quad T = 1, \quad y \to \infty : \partial\psi/\partial y = 0, \quad T = 0 \tag{16}$$

where the parameter $F_0 = C\sqrt{K}\alpha/\nu d$ represents the structural and thermophysical properties of the porous medium, and $Ra = Kg\beta(\overline{T}_w - \overline{T}_\infty)d/\alpha\nu$ is the pore diameter dependent Rayleigh number which describes the relative intensity of the buoyancy force, and d is the pore diameter.

It is noteworthy that $F_0 = 0$ corresponds to the Darcian free convection regime and $\gamma = 0$ represents the case where the thermal dispersion effect is neglected.

Because the dimensionless equations do not depend on the Prandtl number, the equations are valid for any kind of fluid.

The local heat transfer rate at the wall which is the primary interest of the study is given by:

$$q_w = -k_e \frac{\partial\overline{T}}{\partial\overline{y}}\bigg|_{\overline{y}=0} = -(k + k_d)\frac{\partial\overline{T}}{\partial\overline{y}}\bigg|_{\overline{y}=0} \tag{17}$$

where k_e [ML/T^3 K] is the effective thermal conductivity of the porous medium which is the sum of the molecular thermal conductivity k and the dispersion thermal conductivity k_d.

Together with the definition of the local Nusselt number:

$$Nu_{\bar{x}} = \frac{q_w}{\overline{T}_w - \overline{T}_\infty}\frac{\overline{x}}{k_e} \tag{18}$$

One can write

$$Nu = -\left[\left(1 + \gamma\frac{\partial\psi}{\partial y}\right)\frac{\partial T}{\partial y}\right]_{y=0} \tag{19}$$

3. Method of solution

In order to solve the non-dimensional governing momentum and energy Eqs. (14) and (15) using the finite element method (FEM), the weak formulations of these equations are derived. It is convenient to prescribe the set of independent test functions to consist of the stream function ψ and the temperature T. To obtain the weak formulation, the governing equations are multiplied by independent weighting functions and then are integrated over the spatial domain with the boundary. Applying integration by parts and making use of the divergence theorem reduces the order of the spatial derivatives and allows for the application of the boundary conditions using the well known Galerkin procedure. This procedure has been implemented using Matlab software.

4. Results and discussion

To gain physical insight, the system of partial differential Eqs. (14) and (15) along with the boundary conditions (16), are solved by finite element method as explained above. Numerical computations are carried out for $1 \leqslant Ra \leqslant 30$, $0 \leqslant F_0 \leqslant 2$ and $\gamma = 0.0, 0.1,$

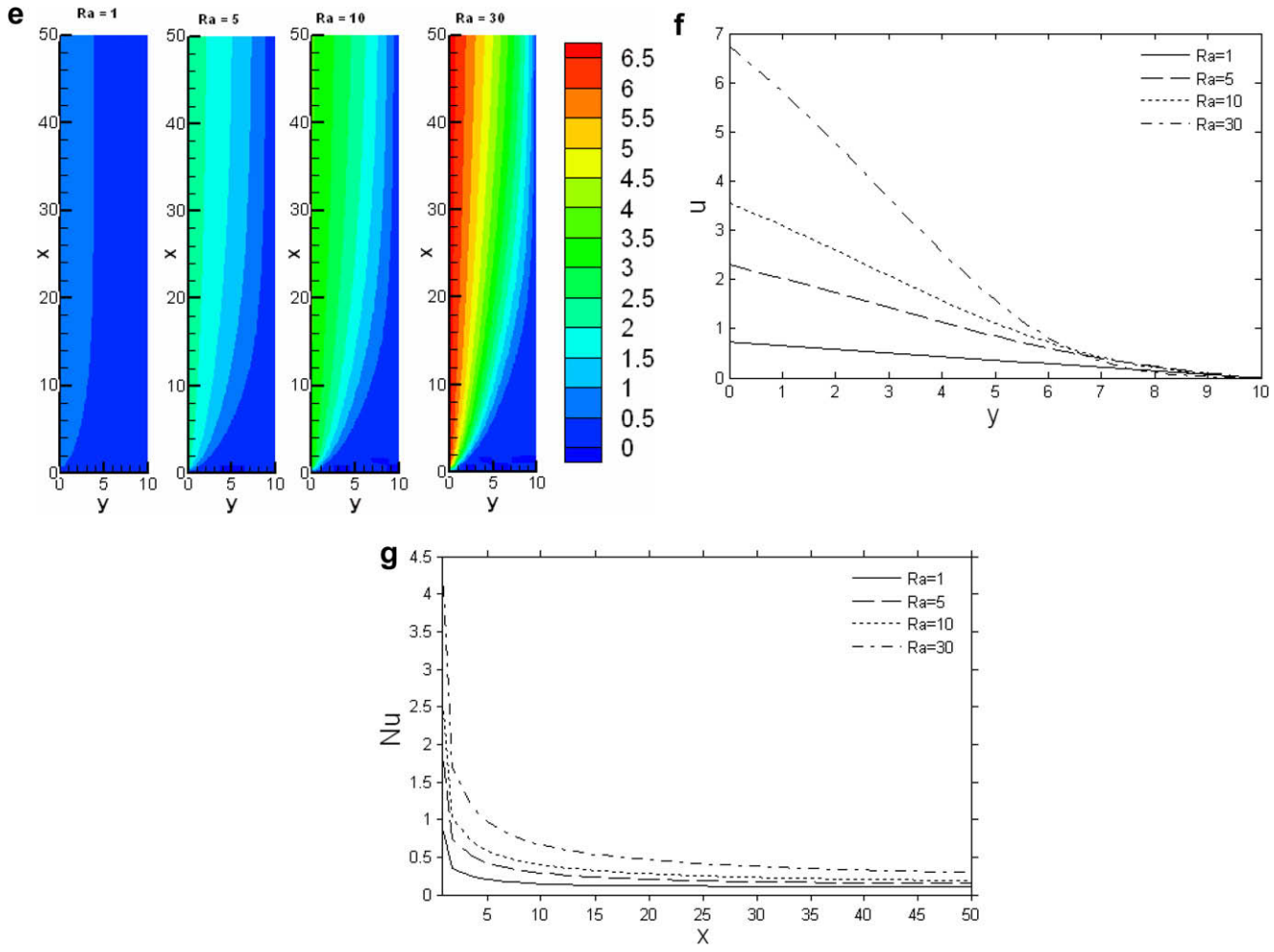

Fig. 2 *(continued)*

0.3.. Table 1 presents an analysis of grid effects. The grid size has been refined until the values of ψ and T stabilize. Further refinement of mesh size over 70×70 elements does not change the values considerably. Thus, elements with $x = y = 10/70$ were used for this study.

4.1. Effects of Rayleigh number

In Fig. 2a, temperature contours for various values of *Ra* are plotted. From this figure, it can be seen that the thermal boundary layer thickness is reduced as *Ra* increases. Rayleigh number describes the relative intensity of buoyancy forces. Thus when *Ra* increases the relative intensity of the buoyancy force increases, consequently, the thickness of the thermal boundary layer is reduced. That is the buoyancy induced upward flow adjacent to the vertical plate increases as the *Ra* increases and is, hence, capable of transporting more heat energy from the wall resulting in a reduction in thermal boundary layer thickness. In other words, heat energy does not have enough time to build up the temperature normal to the vertical wall. This is further illustrated in Fig. 2b which shows the temperature distribution at $x = 10$ for varies values of *Ra*, with the same set of parameters set constant, as a function of the boundary layer thickness. It is notable that as *Ra* increases the temperature distribution normal to the wall decreases and confines towards the wall indicating a reduction in thermal boundary layer thickness.

Fig. 2c shows the contours of the stream function for various values of *Ra* with the following parameters set constant as: $F_0 = 0.5$ and $\gamma = 0.3$. It is observed from this figure that the stream functions, which are related to the volume flow rate per unit thickness, increases as *Ra* increases. That is more flow is induced towards the wall with the increase in *Ra* as explained earlier. This is also supported by looking at Fig. 2d that describes stream function distribution for varies values of *Ra* for the same set of parameters as a function of the boundary layer thickness (cross section at $x = 10$). One notes that as *Ra* increases the stream function increases.

Fig. 2e shows the contours of the vertical velocity field for varies values of *Ra* at $F_0 = 0.5$ and $\gamma = 0.3$, in which one can notice that the velocity of the fluid adjacent to the wall increases with the increase

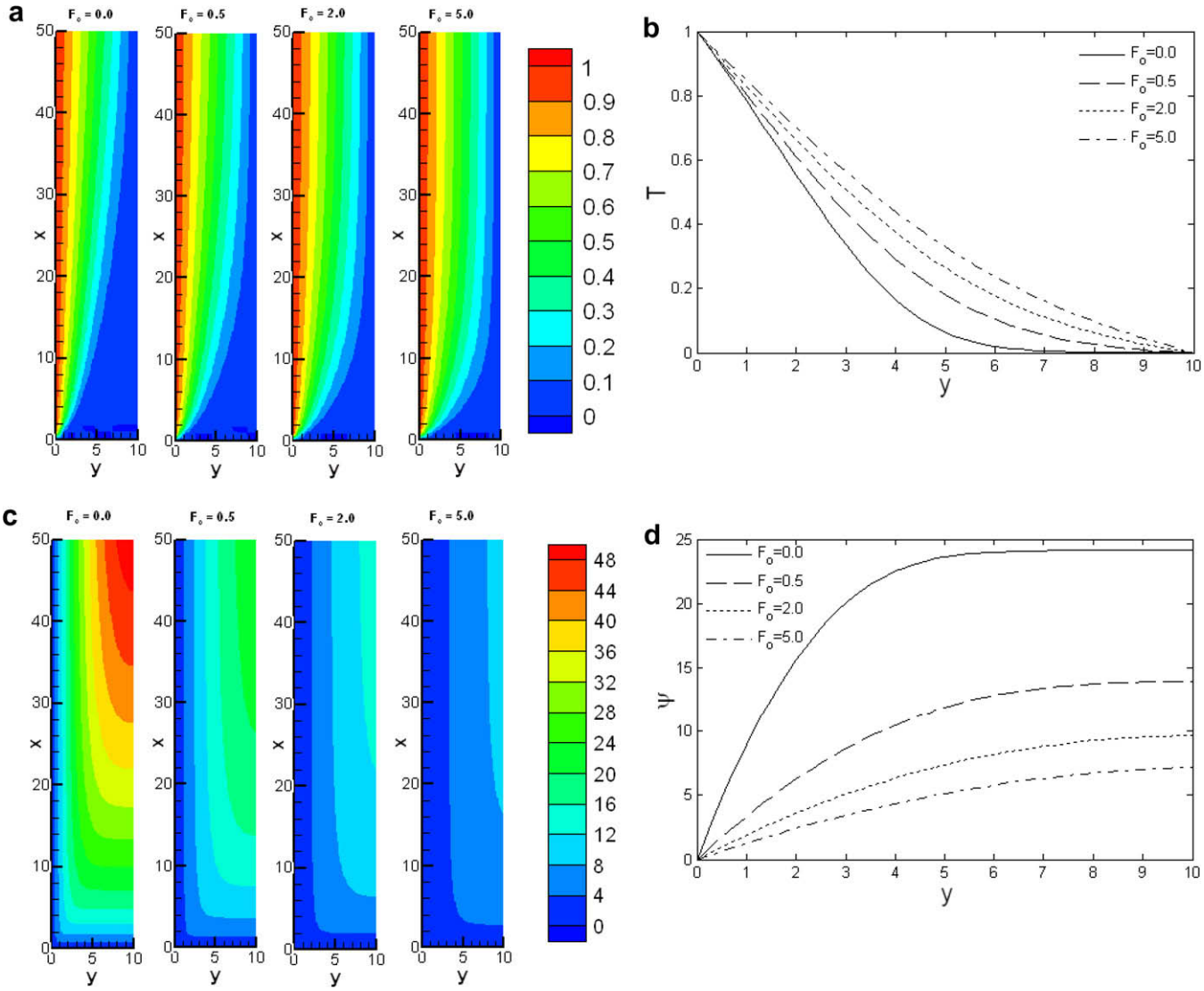

Fig. 3. (a) Temperature contours for various values of F_0 at $Ra = 10$ and $\gamma = 0.3$. (b) Temperature profiles for various values of F_0 at $Ra = 10$ and $\gamma = 0.3$ at $x = 10$. (c) Stream function contours for various values of F_0 at $Ra = 10$ and $\gamma = 0.3$. (d) Stream function profiles for various values of F_0 at $Ra = 10$ and $\gamma = 0.3$ at $x = 10$. (e) Velocity contours for various values of F_0 at $Ra = 10$ and $\gamma = 0.3$. (f) Velocity profiles for various values of F_0 at $Ra = 10$ and $\gamma = 0.3$ at $x = 10$. (g) Nusselt number as a function of x for various values of F_0 at $Ra = 10$ and $\gamma = 0.3$.

in Ra. This may be attributed to the fact that when *Ra* increases the relative intensity of the buoyancy force increases, consequently, more flow is induced to move upwards and hence the velocity of the fluid increases. On the other hand viscous boundary layer does not seem to significantly be affected by the increase in *Ra* in the range studied. Fig. 2f illustrates the upward velocity distribution for varies values of *Ra* for the same set of parameters as a function of the boundary layer thickness (cross section at $x = 10$). It is noted from this figure that as *Ra* increases the velocity increases. On the other hand, this figure also shows that at *Ra* equals 30, the velocity distribution seems to be falling a bit faster at the edge of the boundary layer than those at lower values of *Ra*. This is believed to be due to the fact that as *Ra* increases and consequently the velocity increases, the boundary layer had less time to grow.

In Fig. 2g, heat transfer rates in terms of Nusselt number for different values of *Ra* and with $F_0 = 0.5$ is plotted as a function of *x*. It is obvious that, an increase in the values of the *Ra* enhances the heat transfer rate, especially when *x* is small, i.e. at the beginning of the construction of the boundary layer, and it drops as *x* increases.

4.2. Effects of the non-Darcy parameter F_0

The non-Darcy parameter, F_0, illustrates the relative importance of the nonlinear drag due to the higher velocities of the fluid in porous media. Thus $F_0 = 0$ implies Darcy regime. Fig. 3a indicates that with the increase in the value of the parameter F_0, the thickness of the thermal boundary layer also increases. This may be due to the decrease in the induced velocity by the effect of the nonlinear drag and hence the thermal boundary layer had enough time to develop. Fig. 3b which shows the temperature distribution for varies values of F_0 as a function of the boundary layer thickness (cross section at $x = 10$) also suggests the same conclusion.

Contours of the stream function for various values of F_0 are plotted in Fig. 3c. It is noteworthy that the stream function decreases as F_0 increases. Fig. 3d illustrates the stream function profiles for varies values of F_0 as a function of the boundary layer thickness (cross section at $x = 10$). Also, this figure reports the same fact.

Velocity contours for various values of F_0 are shown in Fig. 3e. It is clear that the momentum boundary layer thickness relatively increases as F_0 increases. Fig. 3f illustrates the velocity profiles for varies values of F_0 as a function of the boundary layer thickness (cross section at $x = 10$). One can note that as F_0 increases the velocity decreases. This figure also shows that the thickness of the momentum boundary layer increases with the decrease in the non-Darcy parameter.

Fig. 3g shows the variation of the heat transfer rate in terms of Nusselt number with F_0 as a function of *x*. It can be seen that, an increase in the values of F_0 reduces the heat transfer rate.

4.3. Effect of thermal dispersion coefficient

In Fig. 4a, the temperature contours for various values of γ are plotted. One can see that the increase in the mechanical dispersion

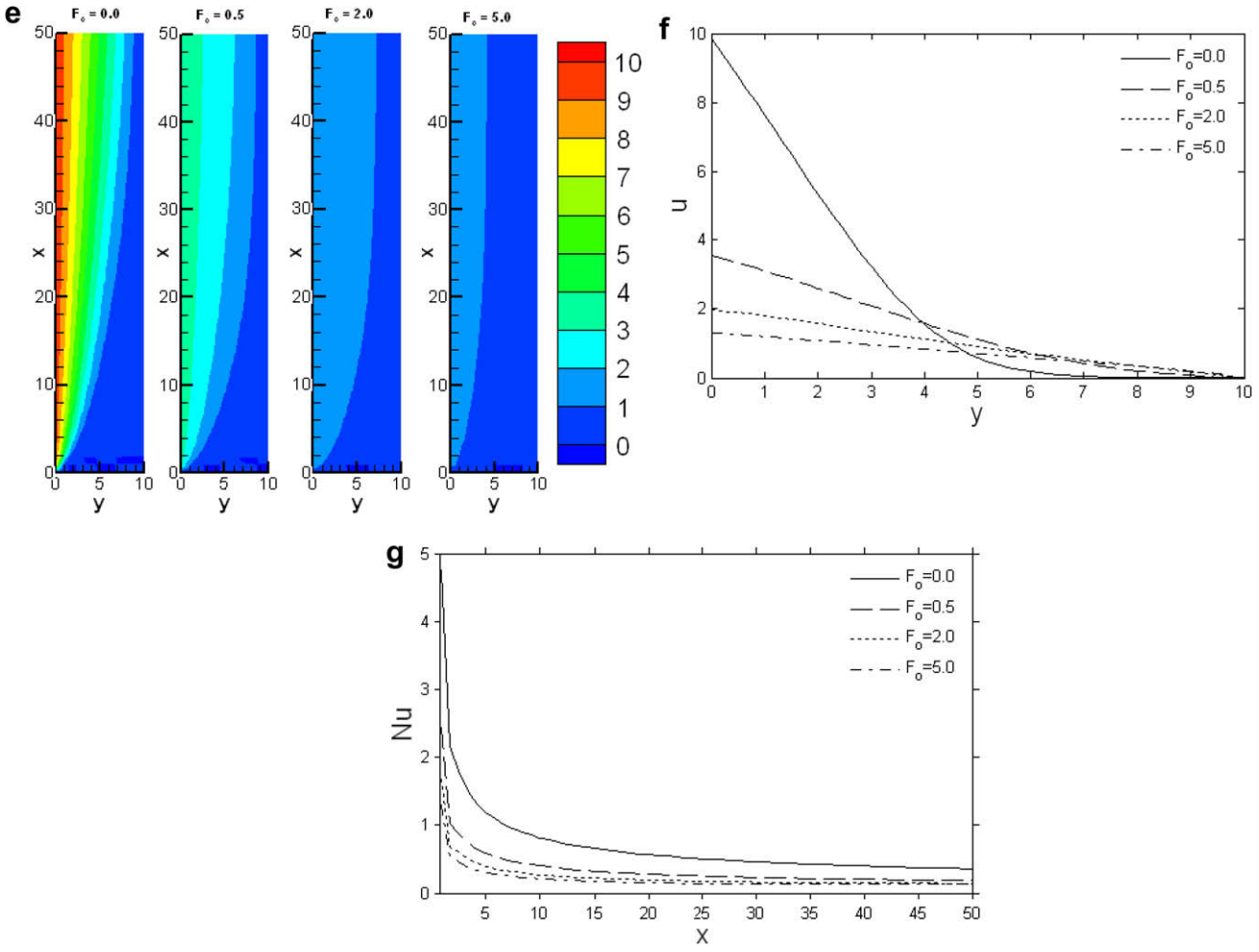

Fig. 3 *(continued)*

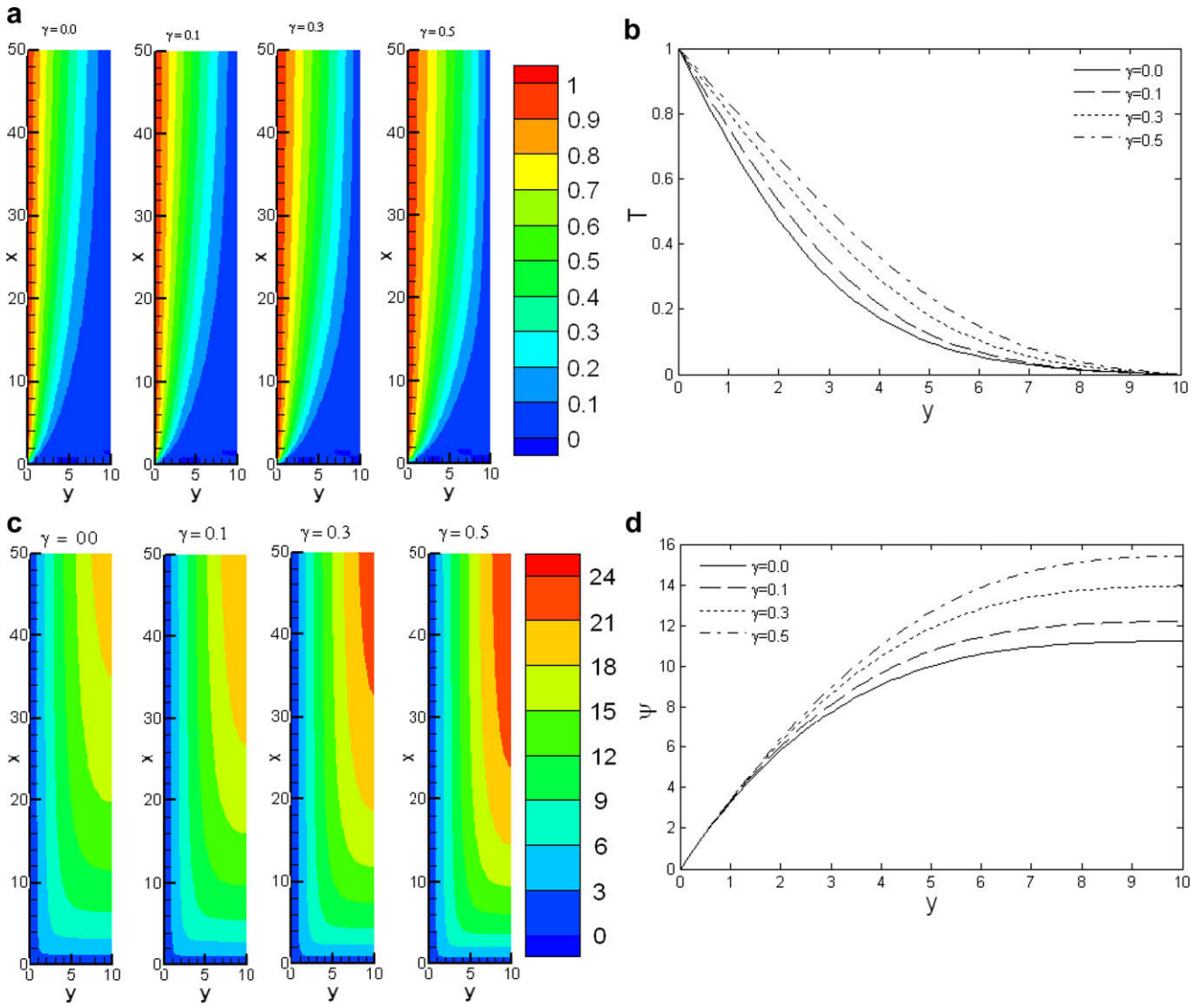

Fig. 4. (a) Temperature contours for various values of γ at $F_0 = 0.5$ and $Ra = 10$. (b) Temperature profiles for various values of γ with $F_0 = 0.5$ and $Ra = 10$ at $x = 10$. (c) Stream function contours for various values of γ at $F_0 = 0.5$ and $Ra = 10$. (d) Stream function profiles for various values of γ with $F_0 = 0.5$ and $Ra = 10$ at $x = 10$. (e) Velocity contours for various values of γ at $F_0 = 0.5$ and $Ra = 10$. (f) Velocity profiles for various values of γ with $F_0 = 0.5$ and $Ra = 10$ at $x = 10$. (g) Nusselt number as a function of x for various values of γ with $F_0 = 0.5$ and $Ra = 10$.

coefficient increases the thermal boundary layer thickness. That is thermal dispersion enhances the transport of heat along the normal direction to the wall as compared with the case where dispersion is neglected (i.e. $\gamma = 0$). Fig. 4b illustrates the temperature profiles for varies values of γ as a function of boundary layer thickness at $x = 10$.

Contours of stream function with different values of the parameter γ are presented in Fig. 4c. It is obvious that the stream function increases as γ increases. In Fig. 4d, stream function profiles for varies values of γ as a function of (boundary layer thickness at $x = 10$). The stream function slightly increases as the dispersion parameter increases.

Contours of velocity for different values of the dispersion parameter are illustrated in Fig. 4e. It is notable from this figure that as γ increases the momentum boundary layer thickness increases. Fig. 4f shows the velocity profiles for varies values of γ as a function of (boundary layer thickness at $x = 10$).

Nusselt number as a function of x for various values of γ is plotted in Fig. 4g. From this figure, it can be seen that the increase in the parameter γ slightly enhances the heat transfer rates.

5. Conclusions

The boundary layer approximations have been used to study the effects of thermal dispersion on heat transfer rates from an isothermal heated semi infinite vertical wall immersed in a saturated porous media. Thermal dispersion has shown to enhance the transport of heat energy along the normal direction to the wall. Moreover, the effect of the non-Darcy parameter which describes the relative intensity of the nonlinear drag when the Reynolds number becomes higher has also been investigated. It was shown that the increase in nonlinear drag coefficient reduces the velocity and hence increases both the hydrodynamic and the thermal boundary layer thicknesses.

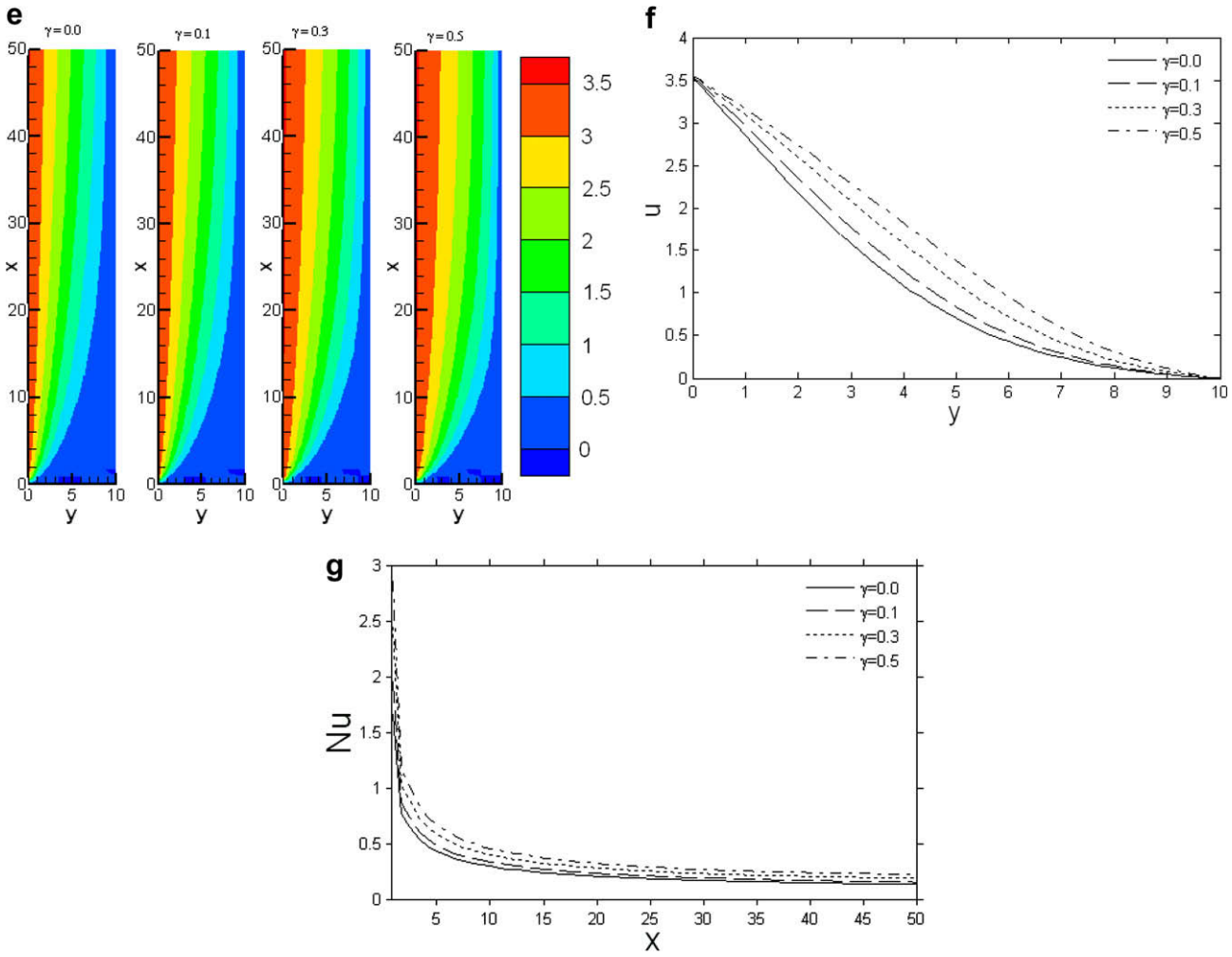

Fig. 4 *(continued)*

In general, this work may be useful in showing that, the use of porous media with better heat dispersion properties may result in better heat transfer characteristics that may be required in many industrial applications (like those concerned with packed bed reactors, nuclear waste disposal, etc.).

References

Cheng, P., 1981. Thermal dispersion effects on non-Darcy convection flows in a saturated porous medium. Lett. Heat Mass Transfer 8, 267–270.

Cheng, P., Minkowycz, W.J., 1977. Free convection about a vertical flat plate embedded in a porons medium with application to heat transfer from a dike. J. Geophys. Res. 82 (14), 2040–2044.

El-Amin, M.F., 2004. Double dispersion effects on natural convection heat and mass transfer in non-Darcy porous medium. Appl. Math. Comput. 156, 1–17.

El-Amin, M.F., 2005. Thermal dispersion effects on non-Darcy axisymmetric free convection in a power-law fluid saturated porous medium. Int. J. Appl. Mech. Eng. 10, 77–86.

Fried, J.J., Combarnous, M., 1976. Dispersion in porous media. Adv. Hydrosc. 11, 169–282.

Georgiadis, J.G., Catton, I., 1988. Dispersion in cellular convection in porous layers. Int. J. Heat Mass Transfer 31, 1081–1091.

Hong, J.T., Tien, C.L., 1987. Analysis of thermal dispersion effect on vertical plate natural convection in porous media. Int. J. Heat Mass Transfer 30, 143–150.

Lai, F.C., Kulacki, F.A., 1989. Thermal dispersion effect on non-Darcy convection from horizontal surface in saturated porous media. Int. J. Heat Mass Transfer 32, 971–976.

Mansour, M.A., El-Amin, M.F., 1999. Thermal dispersion effects on non-Darcy axisymmetric free convection in a saturated porous medium with lateral mass transfer. Int. J. Appl. Mech. Eng. 4, 127–137.

Murthy, P.V.S.N., Singh, P., 1997. Thermal dispersion effects on non-Darcy natural convection with lateral mass flux. Heat Mass Transfer 33, 1–5.

Plumb, O., 1983. The effect of thermal dispersion on heat transfer in packed bed boundary layers. In: Proceedings of First ASME/JSME Thermal Engineering Joint Conference, vol. 2, pp. 17–22.

Salama, A., Van Geel, P.J., 2008. Flow and solute transport in saturated porous media: 1 – the continuum hypothesis. J. Porous Media 11 (4), 403–413.